FORMATION AND CHARACTERISTICS OF COASTAL INTERNAL BOUNDARY LAYERS DURING ONSHORE FLOWS

GILBERT S. RAYNOR, S. SETHURAMAN and ROBERT M. BROWN
Brookhaven National Laboratory, Upton, N.Y. 11973, U.S.A.

(Received in final form 26 January, 1979)

Abstract. The development and characteristics of coastal internal boundary layers were investigated in 28 tests. These were made at all seasons and in both gradient and sea-breeze flows but only during mid-day periods. Measurements of turbulence and temperature were taken from a light aircraft which flew traverses across Long Island at successive altitudes parallel to the wind direction. These were used to locate the boundary between modified and unmodified air as a function of height and distance from the coast. The same measurements plus tower measurements of wind, turbulence and temperature, pilot balloon soundings and measurements of land and water surface temperatures by a remote sensing IR thermometer were used to quantify the characteristics of the modified and unmodified air.

The boundary layer slope was steep close to the land-water interface and became shallower with downwind distance. Growth of the boundary layer was initially slower with stable lapse rates upwind than with neutral or unstable conditions over the water. An equilibrium height was found in many tests except under conditions of free convection when the internal boundary layer merged into the mixed layer inland and with sea-breeze conditions. The equilibrium height depended on downwind conditions and was greater with low wind speeds and strong land surface heating than with stronger winds and small land-water temperature differences. Current theoretical models are not adequate to predict the height of the boundary layer at the altitudes and distances studied but reasonably good predictions were given by an empirical model developed earlier.

Wind speed in the modified air averaged about 70% of that at the coast but turbulence levels were several times higher both near the surface and aloft. These findings have important implications for diffusion from coastal sites.

1. Introduction

One of the most important and characteristic features of the atmospheric environment in coastal regions is the internal boundary layer formed when air flows across the surface discontinuity between land and water. Since the two surfaces rarely have the same temperature and almost always differ in aerodynamic roughness, an interface is created. This typically starts at the surface discontinuity and slopes upward in the direction of the flow at a rate dependent on wind speed, the original characteristics of the air and the properties of the downwind surface.

Coastal boundary layers may be primarily caused by differences in surface temperature (thermal boundary layers) or by differences in surface roughness (roughness boundary layers) but are typically caused by differences in both properties. Two situations are of primary interest during onshore flows, land rougher and warmer than the water and land rougher and colder than the water. Cases with the two surfaces at the same temperature are rare and of brief duration while cases with land smoother than water seldom exist. Analogous situations occur for offshore flows.

Boundary Layer Meteorology **16** (1979) 487–514. 0006–8314/79/0164–0487$04.20.

Many power plants, industrial complexes, nuclear reactors and other potentially polluting installations are located in coastal zones because of proximity to population centers, access to transportation facilities and availability of cooling water. Therefore, both sources and receptors are more numerous and often closer together at coastal than at inland locations. Thus, the potential for adverse effects is higher while the problems of predicting diffusion and in meeting air pollution standards and safety requirements are more acute. In fact, current ability to predict diffusion and resulting concentrations from sources near coastlines is severely limited by inadequacies of the models available and by lack of experimental data on coastal boundary-layer formation and characteristics.

Coastal boundary layers were discussed and the data available at the time summarized in reviews by Prophet (1961) and van der Hoven (1967). Echols and Wagner (1972) studied the lower levels of a boundary layer on the Texas coast. De Vecchio *et al.* (1976) evaluated the performance of a formula presented earlier by Raynor *et al.* (1975) for predicting boundary-layer height. Hewson and Olsson (1967), Lyons and Olsson (1972), Lyons and Cole (1973), Collins (1974) and Dooley (1976) studied air pollution problems associated with coastal boundary layers. Effects on atmospheric diffusion of meteorological processes in coastal zones were described by Raynor (1977). This paper reports recent experimental studies of boundary-layer development and describes the characteristics of the air within and outside of the boundary layer. This study is part of a comprehensive investigation of meteorology and diffusion in a coastal environment (Raynor *et al.*, 1975, 1978).

Boundary-layer development has also been treated theoretically. Modifications in the wind field due to changes in surface roughness have been studied by Elliot (1958) and Panofsky and Townsend (1964). Several numerical models exist that treat the airflow above changes in surface heat flux, temperature and roughness in varying degrees of sophistication and detail (Peterson, 1969; Taylor, 1969a, 1969b, 1969c, 1970, 1971). Peterson (1969) assumed that the horizontal shear stress is proportional to the turbulent energy and neglected the influence of pressure changes. Using the horizontal momentum, continuity and energy equations, with some boundary conditions, internal boundary-layer development due to a change in roughness was computed for neutral conditions. Taylor (1969c) also used horizontal momentum and continuity equations but with the "mixing-length" hypothesis to predict the modification in airflow due to a change in surface roughness for neutral conditions. Taylor in a later analysis (1970) included a change in surface temperature and developed a numerical model based on horizontal momentum, heat and continuity equations with a mixing-length hypothesis. The Businger-Dyer hypothesis for the non-dimensional wind shear and heat flux was used. Neutral upwind and unstable downwind conditions were studied with both increase and decrease in surface roughness. The above numerical model was extended by Taylor (1971) to include downwind stable atmospheric conditions. These models essentially treat the growth of the internal boundary layer to a height of 100 m within the surface layer of the atmosphere. This restricts these models to short distances from the surface

discontinuity. No theoretical or numerical model is found in the literature that treats the growth of an internal boundary layer with stable conditions upwind and unstable conditions downwind, conditions which characterized most of the tests described in this paper.

2. Experimental Methods

Coastal boundary-layer development was studied primarily by instrumented aircraft flights across the width of Long Island during periods of air flow from ocean to land. Flights were made at selected altitudes along tracks shown in Figure 1. Track 3 was

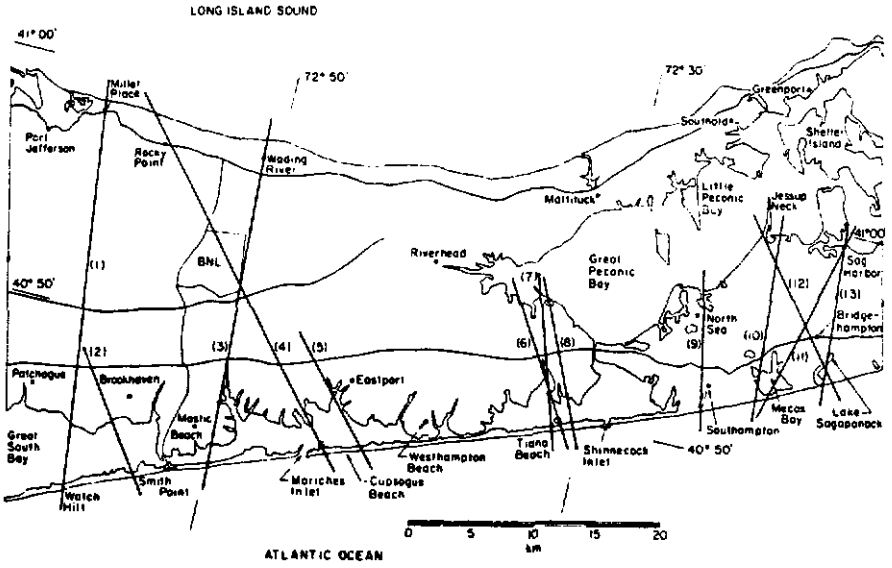

Fig. 1. Map of central Long Island showing flight tracks used (1–13), location of Brookhaven National Laboratory (BNL) and measurement sites at Smith's Point and Tiana Beach.

used most frequently since it and track 1 were used specifically for these studies. The other tracks were used during diffusion tests in which measurement of the boundary layer was only one of many activities (Raynor *et al.*, 1975). Boundary-layer flights were usually made in mid-day when conditions were changing least since a full set of measurements took several hours. On some sea breeze days, a less extensive set of measurements was made early in the morning to document conditions before the onset of the sea breeze. A list of tests with associated weather conditions and data taken is given in Table I. In the table, grad. means gradient wind and SB a sea breeze flow. Wind speeds were taken at a height of 11 m. Lapse rates are for the height interval from 152–305 m since few measurements were obtained below 152 m. Quite different results could be obtained in some cases by choice of different height intervals or by using sea surface temperature for the lowest layer.

TABLE I

Description of tests with weather conditions and data obtained

Test No.	Date	Time (EST)	Weather	Flow	Wind direction (deg)		Wind speed ($m\ s^{-1}$)		Surface Temp. (°C)		Lapse Rate (°C/100 m)		Data taken					
					Coast	Inland	Coast	Inland	Ocean	Land	Ocean	Land	Turbulence σ_w	Turbulence ε	Temp. Aloft	Winds Aloft	IR Temps.	Tower Temps.
W1	5-17-73	1300–1431	○	grad. + SB	138	150	5.8	5.3	—	—	−0.78	−1.44		×	×			
S6	5-23-73	1130–1234	⊕Sc, R−	grad.	125	113	4.6	1.9	12.3–13.4	—	−0.46	−0.33	×		×	×		
S7	6-1-73	1100–1317	◑Ci, H+	grad.	222	203	7.5	4.6	—	—	−0.52	−0.85	×		×	×		
S9	7-13-73	1100–1200	◑Ci, Sc	grad.	231	223	6.7	5.3	18.0–18.1	—	+0.85	−0.46	×		×	×		
S10	9-20-73	1133–1307	◑ Ci, Cu− ◉ Ci, Ac, Cu	grad.	231	194	8.5	3.8	18.5	—	−0.85	−1.11	×		×	×		
W5	12-4-73	1220–1335	○	grad.	235	184	5.1	3.8	9.0–10.7	—	+1.73	+1.57	×		×	×		
W6	1-23-74	1325–1420	○ –◑Ci	grad.	240	204	7.7	4.5	5.8	—	+0.45	−0.45	×		×	×		
W7	2-28-74	1105–1452	⊕Ci, Cs, As− ◑Ci, Cs	grad.	232	204	6.8	5.5	4.3	—	−0.91	−0.72	×		×	×		
S11	4-11-74	1110–1435	◑Ci–◑Ci, Cs	grad.	232	219	7.8	1.2	6.2	—	−0.13	−0.98	×		×	×		
S12	5-14-74	1025–1255	◑Ci–○, H	grad.	211	202	6.9	6.5	11.1–11.9	—	−0.20	−0.98	×		×	×		
BL1	6-5-74	1245–1531	◑–⊕Ci	grad.	215	209	5.4	4.5	—	—	+1.31	−0.72	×		×	×		×
S13	6-14-74	1105–1950	◑Ci,	grad.	145	151	3.6	2.6	17.1–17.4	—	−0.39	—	×		×	×	×	
BL2	6-19-74	1134–1522	◑Ci, Cu− ⊕Ci—◑Ci	SB	198	192	6.0	4.0	—	—	−0.52	−0.72	×		×	×		×
BL3	7-2-74	1156–1613	○–◑Ci	SB	218	204	7.0	5.2	—	—	−0.02	−0.72	×		×	×		×
BL4	7-9-74	1112–1500	◑Ci, H	grad.	242	305	6.4	4.0	—	—	−0.65	−1.01	×		×	×		×
S14	7-18-74	1100–1235	⊕As, Ac, H+	grad.	203	197	9.1	4.0	20.1–21.2	—	−0.07	−0.46	×		×	×		
BL5	8-1-74	1143–1607	◑Cu	SB	215	214	6.3	4.8	—	—	−0.49	−0.88	×		×	×		×
W9	8-16-74	1005–1506	◑Ci, Cu	SB	150	195	5.0	3.7	19.4–20.8	25.5–34.0	−0.11	−0.85	×		×	×		
S15	3-6-75	1015–1158	◑Ci, Ac− ⊕As, Ac	grad.	167	166	8.7	7.2	2.5–4.9	—	−0.88	−0.87	×		×	×	×	
BL6	3-18-75	0928–1356	○–◑ Ci, Cu	grad.	100	122	4.5	4.0	8.3	14.0–20.0	−1.31	−0.91	×		×	×	×	×
BL7	5-21-75	1235–1512	◑V⊕ As, Ac, Cu, H+	grad. + SB	240	192	4.3	2.2	14.6–18.0	33.0	+0.20	−1.01	×		×	×	×	×
W11	6-23-75	1200–1346	○, H	grad.	225	229	6.8	3.7	15.3–18.1	—	−0.19	−0.65	×		×	×	×	
BL8	11-12-75	1032–1425	○–⊕ As, Sc, RW−	grad.	157	163	6.1	3.9	15.8–17.0	16.4–18.0	−0.95	−0.98	×		×	×	×	×
BL9	3-19-76	1244–1552	◑Ci–⊕Ci, Cs	grad.	207	203	7.2	5.2	3.0–4.0	12.5–20.0	+2.16	−0.52	×		×	×	×	×
W29	6-11-76	1155–1440	○, H+	grad. + SB	221	197	5.5	3.6	13.5–16.6	31.0	+1.14	+0.39		×	×	×	×	
W30	6-14-76	1148–1450	⊕ As, H	grad.	205	208	5.6	5.0	14.5–15.6	25.0	+0.04	−0.95		×	×	×	×	
BL10	6-24-76	1155–1457	◑Cu, Cb	SB	203	208	7.2	4.4	17.4–17.9	29.0–36.0	−0.36	−0.98		×	×	×	×	
BL11	7-27-76	0936–1253	◑ Ci, Sc, Ac− ◑ Ci, Cs	grad. + SB	209	213	7.4	2.9	19.3–20.6	25.2–30.0	−0.56	−1.11		×	×	×	×	

Two single-engine Cessna aircraft were used in boundary-layer flights. One carried a Ball Model 101-B electrical variometer for measuring turbulence and made horizontal traverses at successive altitudes from about 1.5 km over the ocean south of Long Island to 1.5 km over Long Island Sound north of the island. The variometer was previously calibrated by flights past an instrumented tower (SethuRaman *et al.*, 1978). Traverses usually started at 152 or 183 m above sea level and extended to 610–914 m in 91-m height intervals. If the maximum height of the boundary layer was reached, additional levels were not flown. In some runs, when time permitted, second traverses were made at one or more levels to document temporal changes which were typically small. In several tests, additional traverses were made parallel to the coastline, completely over water or over land. These did not intersect the boundary and are not included in the results presented here.

In the last four flights, a MRI Universal Indicated Turbulence System Model 1120 (Epsilon Meter) was used in place of the variometer to measure the energy

TABLE II

Description of boundary-layer turbulence flights

Test No.	Date	Time (EST)	Track	Height (m)		Levels	Instrument
				Minimum	Maximum		
W1	5-17-73	1300–1431	8	152	610	4	Variometer
S6	5-23-73	1130–1234	6	152	610	4	Variometer
S7	6-1-73	1100–1317	7	183	944	10	Variometer
S9	7-13-73	1100–1200	8	183	580	5	Variometer
S10	9-20-73	1133–1307	7	152	914	6	Variometer
W5	12-4-73	1220–1335	7	152	458	5	Variometer
W6	1-23-74	1325–1420	7	152	610	6	Variometer
W7	2-28-74	1105–1452	2,3,5 & 8	183	610	9	Variometer
S11	4-11-74	1110–1435	9	213	610	5	Variometer
S12	5-14-74	1025–1255	13	152	701	7	Variometer
BL1	6-5-74	1245–1531	3	152	792	8	Variometer
S13	6-14-74	1105–1350	12	152	762	7	Variometer
BL2	6-19-74	1134–1522	3	152	792	8	Variometer
BL3	7-2-74	1156–1613	3	152	792	8	Variometer
BL4	7-9-74	1112–1500		152	792	8	Variometer
S14	7-18-74	1100–1235	13	152	701	7	Variometer
BL5	8-1-74	1143–1607	1 & 3	152	792	8	Variometer
W9	8-16-74	1005–1506	13	152	610	6	Variometer
S15	3-6-75	1015–1158	10	152	610	6	Variometer
BL6	3-18-75	0928–1356	4	183	914	9	Variometer
BL7	5-21-75	1235–1512	3	183	914	9	Variometer
W11	6-23-75	1200–1346	11	152	579	6	Variometer
BL8	11-12-75	1032–1425	3	183	914	9	Variometer
BL9	3-19-76	1244–1552	3	183	732	7	Variometer
W29	6-11-76	1155–1440	3	183	274	2	ε meter
W30	6-14-76	1148–1450	13	183	732	7	ε meter
BL10	6-24-76	1155–1457	3	183	914	9	ε meter
BL11	7-27-76	0936–1253	3	183	823	9	ε meter

dissipation rate, ε. In most of the later flights, the aircraft also carried a Barnes PRT-5 infrared remote sensing thermometer for measuring land and water surface temperatures. Turbulence flights are summarized in Table II.

The second aircraft was equipped with a thermistor temperature sensor which was used to measure air temperature during vertical spirals at nine equally spaced locations along the same track and over a similar height interval as that sampled by the first aircraft. Temperature readings were taken at 30-m height intervals. Because of the lesser time needed, two complete sets of temperature measurements and sometimes another partial set were taken during the time needed for one complete set of turbulence measurements. Temperature flights are summarized in Table III. Altitudes below 152 m were measured only over water.

TABLE III

Description of boundary-layer temperature flights

Test No.	Set No.	Time (EST)	Track	No. locations	Height (m)	
					Minimum	Maximum
W1	1	1300–1320	8	2	61	762
S6	1	1130–1200	8	2	91	914
S7	1	1145–1200	8	2	91	914
S9	1	1100–1125	8	2	152	914
S10	1	1145–1210	8	2	152	914
W5	1	1220–1250	8	2	152	762
	2	1325–1335	8	1	152	762
W6	1	1325–1355	8	2	152	762
W7	1	1110–1135	8	2	152	914
	2	1315–1325	2	1	152	914
S11	1	1110–1135	8	2	152	762
	2	1425–1435	8	2	152	762
S12	1	1025–1045	8	2	61	762
	2	1200–1255	13	4	152	762
BL1	1	1244–1423	3	6	114	876
S13	1	1105–1115	8	1	31	762
BL2	1	1134–1253	3	9	152	914
	2	1309–1422	3	9	152	914
	3	1435–1442	3	1	152	914
BL3	1	0727–0836	3	2	152	2256
	2	1204–1311	3	9	46	914
	3	1326–1424	3	9	46	914
	4	1442–1458	3	2	46	914
BL4	1	0604–0654	3	2	152	2438
	2	1115–1236	3	9	152	914
	3	1247–1400	3	9	152	914
	4	1433–1500	3	3	152	914
S14	1	1100–1110	8	1	61	762
	2	1114–1146	13	4	152	762
BL5	1	0615–0640	3	2	30	914
	2	1145–1253	3	9	152	914
	3	1312–1410	3	9	152	914
	4	1417–1435	3	2	152	914

TABLE III (*continued*)

Test No.	Set No.	Time (EST)	Track	No. locations	Height (m)	
					Minimum	Maximum
W9	1	1005–1010	8	1	152	914
	2	1315–1320	8	1	30	914
	3	1330–1401	3	4	30	914
S15	1	1015–1030	8	2	152	914
	2	1135–1158	10	4	152	762
BL6	1	0928–1047	3	9	152	914
	2	1145–1356	3	9	152	1067
BL7	1	0630–0700	3	2	152	914
	2	1235–1357	3	9	152	914
	3	1402–1512	3	9	152	914
W11	1	1200–1220	8	2	122	914
BL8	1	1032–1155	3	9	152	914
	2	1257–1425	3	9	152	914
BL9	1	1244–1358	3	9	152	914
	2	1441–1552	3	9	152	914
W29	1	1155–1220	8	2	30	762
	2	1317–1325	8	1	30	762
	3	1432–1440	8	1	91	762
W30	1	1148–1206	8	2	30	762
	2	1241–1325	11	4	30	762
	3	1440–1450	8	1	30	762
BL10	1	1155–1321	3	9	152	914
	2	1330–1457	3	9	152	914
BL11	1	0936–1054	3	9	152	914
	2	1139–1253	3	9	152	914

In flights during diffusion tests, only one aircraft was used. Thus, the number of temperature spirals and horizontal traverses was usually less although each traverse was quicker since the shorter tracks (6–13) across the south fork of Long Island were used. However, most of these flights gave data adequate for delineating the boundary layer.

During boundary-layer flights, pilot balloon soundings were taken every half hour at Brookhaven National Laboratory (BNL) and Smith's Point (Figure 1). During diffusion tests, soundings were taken at less frequent intervals from Tiana Beach (Figure 1). In most runs, air temperature was recorded at three levels of the 128-m meteorology tower at BNL.

Low-level turbulence in and out of the boundary layer was measured with MRI bivanes operated simultaneously at a height of 23 m on the tower at BNL and on a tower at Tiana Beach during onshore flows. Data were recorded on magnetic tape recorders. Mean wind speed and direction differences were documented by simultaneous strip chart recordings from Bendix-Frieze aerovanes at two coastal and two inland sites.

3. Analytical Methods

During early tests, turbulence measurements aloft were recorded on a strip-chart recorder. Turbulence as a function of location and height was classified by the width of the trace and the frequency of the fluctuations into relative classes from very light to very heavy. Results were plotted as vertical cross-sections along the track of the flights. From these plots and the temperature cross-sections, the location of the boundary between modified and unmodified air, the slope and the equilibrium height were determined. In later runs, data were taken on a TEAC tape recorder as well as on the chart recorder. The taped data were used to compute σ_w, the vertical component of the turbulent fluctuations. Values of σ_w were classified as a function of height and location with respect to the boundary layer (Figure 2).

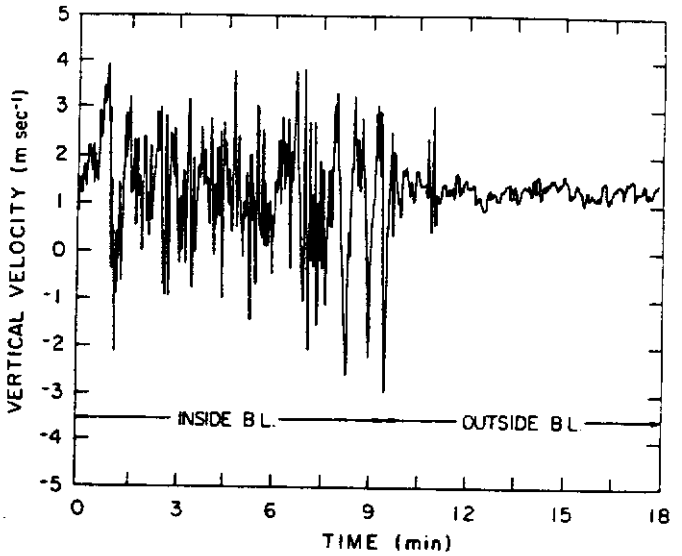

Fig. 2. Vertical velocity (σ_w) inside and outside of the internal boundary layer (B.L.)

Aircraft temperature data were plotted as profiles at each location and as vertical cross-sections along the track of the flight. These cross-sections were used with the turbulence cross-sections to locate the boundary layer and to illustrate air modification over the land. Both turbulence and temperature data were used in defining sea-breeze circulations.

Wind speed and direction from pilot balloon soundings were plotted as a function of height. The plots were used to show differences between the coastal and the inland location and to document temporal changes.

The infrared surface temperature data were tabulated and the differences between land and water were used with other data to test the formula developed earlier (Raynor *et al.*, 1975) to predict the height of the boundary layer.

Bivane data were analyzed to determine the mean and standard deviation of the turbulent fluctuations in the three component directions. Results were used to characterize the modified and unmodified air.

Mean wind speed and direction data from coastal and inland sites were used to document changes in direction and decreases in speed as air moved inland from the ocean.

4. Results

4.1. Turbulence cross-sections

The coastal boundary layer is best defined by the intensity of turbulence as plotted in vertical cross-sections along the path of the flight. Since turbulence is related to both temperature and roughness of the underlying surface, the boundary layer determined from the turbulence level was usually higher than that determined from the temperature field alone. This agrees with wind-tunnel studies (SethuRaman and Cermak, 1975).

A typical case (Run S13) is illustrated in Figure 3. These measurements were made along track 12 across the south fork of Long Island on a sunny day in June with light wind speeds. The boundary is quite steep with a gradual transition from light turbulence over the ocean to heavy turbulence over the land. Equilibrium height is above 700 m. The beginning of another boundary layer over the water to the north may be indicated by the moderate turbulence at low levels.

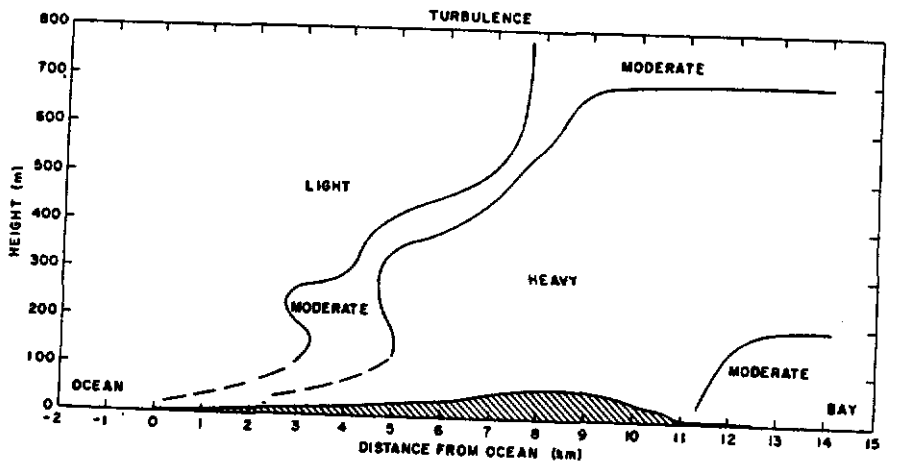

Fig. 3. Turbulence cross-section during run S13 with light wind speeds and clear skies.

In contrast, Figure 4 illustrates a flight (Run S14) along track 13 on a July day with middle overcast and rather strong wind speeds. The slope is shallower, the equilibrium height below 400 m and the transition from light to heavy turbulence quite abrupt. The heavy turbulence extends out over the bay to the north down to the lowest measuring level.

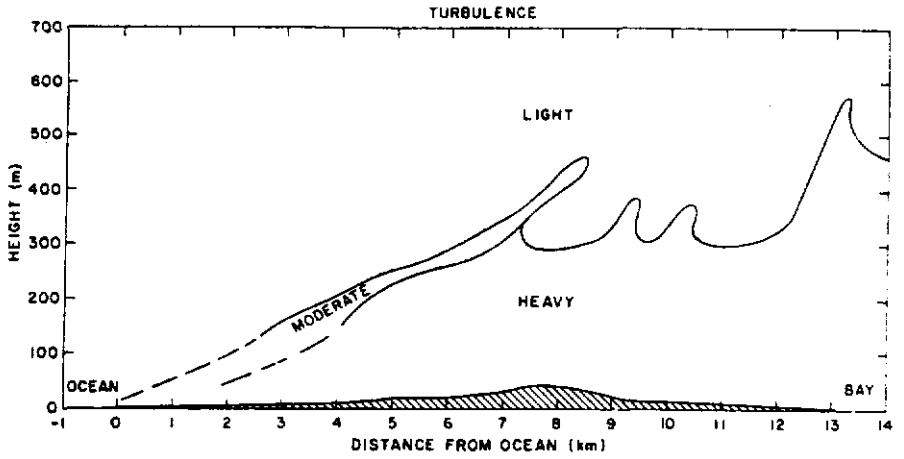

Fig. 4. Turbulence cross-section during run S14 with strong winds and overcast skies.

The turbulence pattern during a strong sea-breeze flow (Run BL5) is illustrated by measurements taken along track 3 across the width of Long Island (Figure 5). Skies were mostly clear and wind speeds moderate. The slope is steep but the transition from light to heavy turbulence gradual. An equilibrium height was not reached and probably did not exist. The heavy turbulence forms a chimney-like pattern marking the air rising at the sea-breeze front. Since the northern portion of Long Island and Long Island Sound were north of the front and in the gradient flow from the west-northwest, the heavy turbulence did not extend over the sound except in the divergence region at the highest levels.

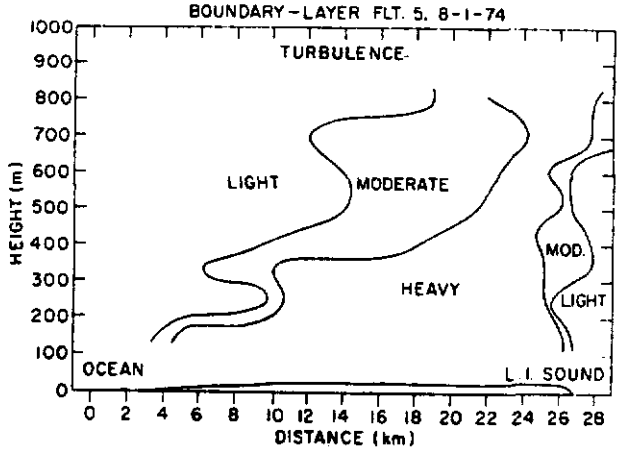

Fig. 5. Turbulence cross-section during a strong sea breeze flow (BL5) showing a chimney of heavy turbulence at the sea breeze front.

A case without onshore flow and with no boundary-layer development (Run BL4) is illustrated in Figure 6 for comparison. On this day, winds were westerly and nearly parallel to the length of the island. An expected sea breeze failed to develop as a changing synoptic pattern strengthened the gradient flow during the midday hours. Heavy turbulence was found across the width of the island with light turbulence over the water on both sides and a transition zone of moderate turbulence.

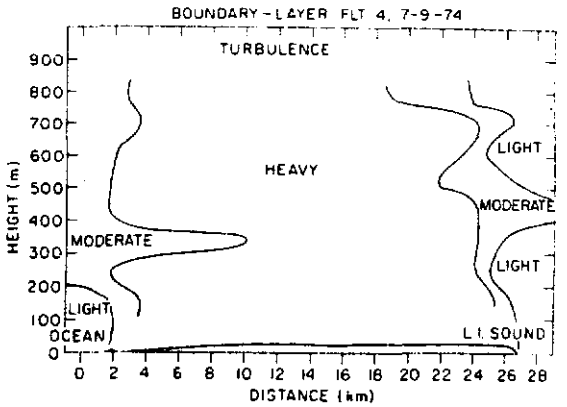

Fig. 6. Turbulence cross-section without internal boundary layer development during flow parallel to Long Island, (BL4).

4.2. Slope

Average slope of the internal boundary layer was determined primarily from the turbulence cross-sections. For each run, a single point was chosen along the top of the boundary layer as far inland as possible before an equilibrium height was reached or any substantial irregularity in the slope occurred. The height at this point and the distance to the coast along the direction of the mean wind were determined. The purpose of taking only one point along each slope was to give equal weight to each case. The alternative procedure of taking points at successive distances along each slope would have given greatest weight to the cases with the largest slopes. In cases when the wind was not normal to the coastline, the distance along the wind was often substantially greater than the distance along the track flown. Distances were taken to the ocean although many along-wind tracks included appreciable distances over the shallow bays inside of the barrier beach (Figure 1). However, the effect of the bays on boundary-layer development could not be determined from the data since the aircraft flight levels were too high to measure the lower portions of the boundary-layer slopes and no other means were available.

The height of the boundary layer at the selected point was divided by the distance from the coast (fetch) to determine the average slope. Values of fetch and slope are given in Table IV. Inspection of the table shows that the shallowest slopes tend to occur with the largest fetches. This indicates that slopes are steepest close to the

TABLE IV

Slope of boundary layer at indicated fetch

Test no.	Fetch (km)	Slope
W1	13.6	0.044
S7	13.1	0.030
S9	7.8	0.038
S10	12.3	0.049
W5	17.3	0.016
W6	24.0	0.017
W7	16.6	0.027
S11	6.5	0.023
S12	13.4	0.033
BL1	22.8	0.021
S13	7.0	0.074
BL2	16.7	0.042
BL3	34.6	0.022
BL4	5.8	0.034
S14	6.6	0.053
BL5	19.0	0.025
W9	4.5	0.071
S15	5.4	0.028
BL6	8.7	0.081
BL7	11.7	0.038
W11	15.2	0.030
BL8	3.7	0.135
BL9	5.4	0.074
W29	17.7	0.016
W30	14.0	0.034
BL10	16.2	0.028
BL11	1.4	0.270

surface discontinuity and flatten with inland distance. This relationship was quantified by plotting the slope as a function of fetch and finding the least-square regression line (Figure 7). The logarithmic relationship shown here had a better correlation coefficient ($r = -0.8111$) than a linear relationship ($r = -0.680$). Figure 7 shows that the average slope varies from about 1:4 at 1 km to about 1:28 at 10 km and less than 1:100 at 50 km. For comparison, four boundary layers illustrated by Dooley (1976) had slopes of from 1:17 to 1:33 at a distance of 10 km from the coast of Lake Michigan. Echols and Wagner (1972) found a slope of 1:13, 90 m inland from the Texas coast.

Slope was next examined to determine how it varied with other conditions. As shown in Figure 8, some difference with season was found although only summer (May–August) and winter (December–March) could be examined since too few cases were obtained in other months. In the winter, slope is greater close to the shore than in summer but less at distances greater than about 12 km. The steeper slope near the discontinuity in winter is believed due to neutral or unstable lapse rates over the

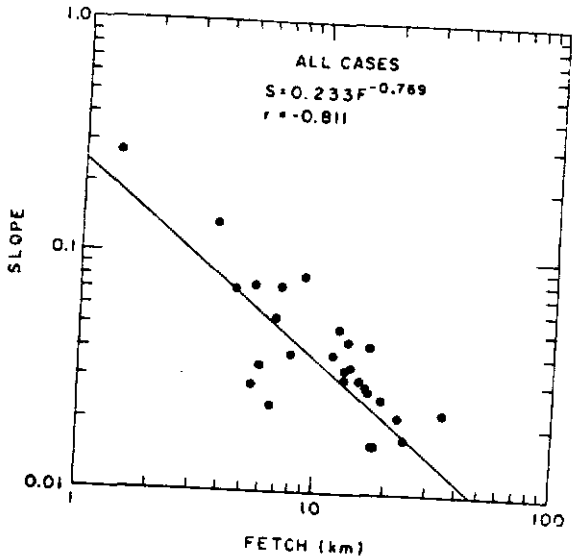

Fig. 7. Change of slope with distance from the land-water interface (fetch) based on one measurement of height and fetch from each test.

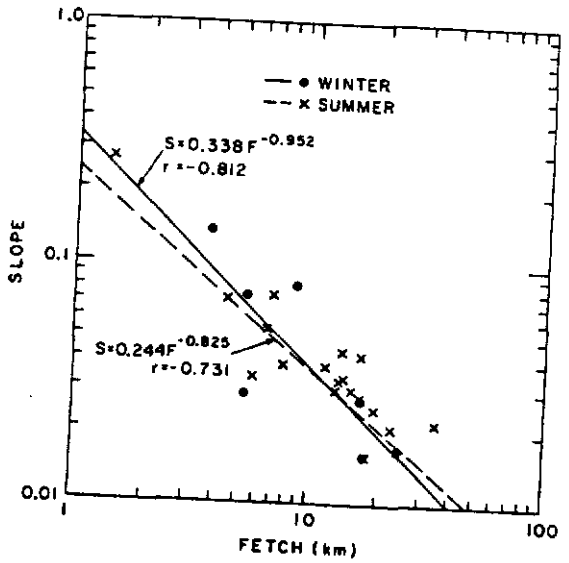

Fig. 8. Change of slope with fetch for winter and summer cases.

ocean. This less stable air is modified more rapidly than the stable air prevailing in summer. At greater distances, the increased heating of the land results in a higher equilibrium level. When the May–June and July–August data were examined separately, the change in slope with distance was fastest in the earlier period when the land-water temperature difference is maximum for the year. Thus, the initial

slope is determined largely by upwind conditions and the equilibrium height by downwind conditions.

A systematic variation of slope with wind speed at the coast was also found (Figure 9). In the first 1–3 km, slope was greatest with high wind speeds and smallest with low speeds but beyond 3 km, the opposite condition occurred. Since winter had a larger percentage of the high wind cases, the slope near the shore may be largely a seasonal effect as discussed above.

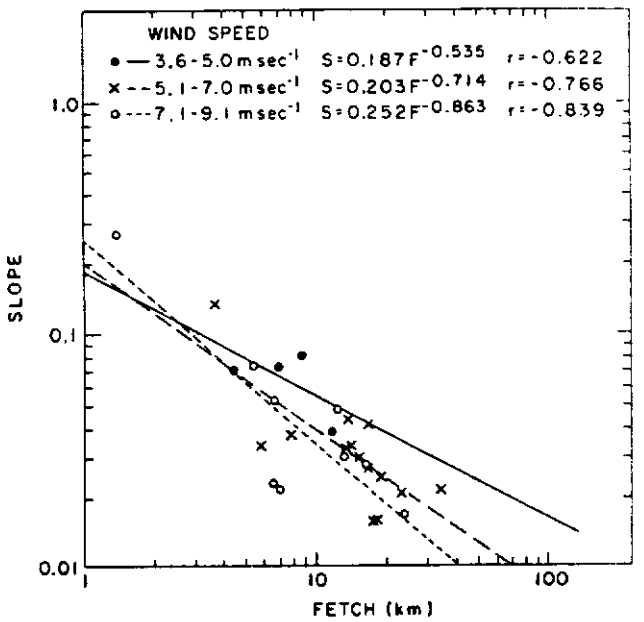

Fig. 9. Change of slope with fetch for three wind speed classes.

Slopes were also examined with respect to cloud cover although tests were not obtained under a wide range of cloud conditions. Under clear skies, change in slope occurred more rapidly than under partly cloudy skies but the differences were not great and equations were not fitted to the data points. Cases were also segregated into sea breeze and gradient flow classes but no significant difference was found between the two groups.

Plots of height *vs.* slope showed considerable scatter so the slope equations were solved for height (h) and mean heights plotted as a function of distance for summer and winter cases (Figure 10). Because the horizontal scale is 100 times the vertical scale on the main plot, the curves for the first 0.5 km are shown on a 1 : 1 scale on the insert graph. Since no actual measurements were made below about 150 m, the details of the lower portions of these curves may not match the slopes in nature. However, the data clearly indicate a steep slope near the surface discontinuity and a decreasing slope, although a continual rise in height, with distance.

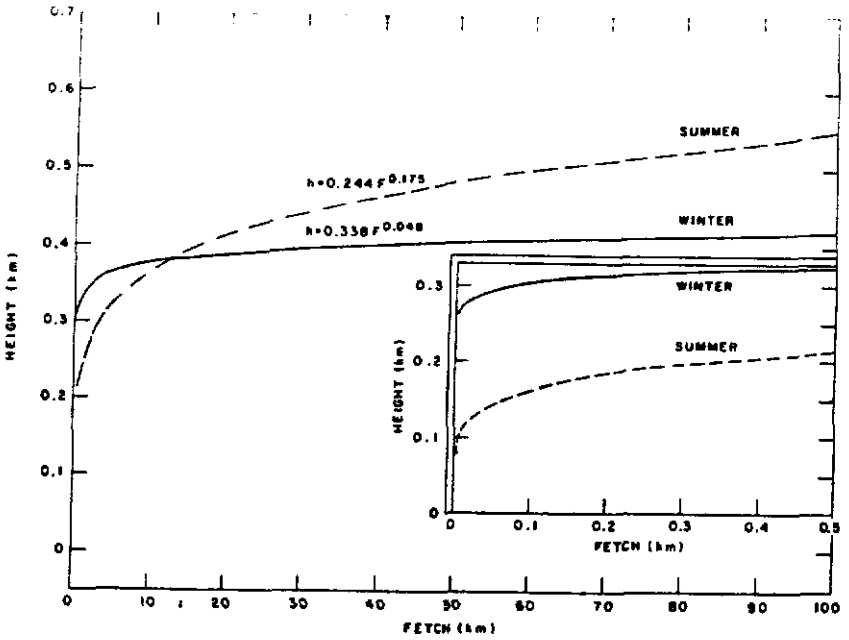

Fig. 10. Change of mean height with fetch for winter and summer cases.

The height of the winter boundary layer (Figure 10) increases rapidly close to the shore while the height in summer rises more slowly as pointed out earlier. At distances beyond 12 km, however, height in summer exceeds that in winter as expected from greater surface heating over the land.

Height is plotted for three wind-speed classes in Figure 11 which shows the effect of increasing wind speed in suppressing the height of the boundary layer except in the first few kilometers where the position of the curves is reversed probably due to seasonal effects.

4.3. Test of Model

Raynor *et al.* (1975) presented the following empirical model derived from physical and dimensional reasoning for predicting the height of a boundary layer from pertinent meteorological data and showed good agreement between predicted and measured heights over the ocean after long overwater fetches.

$$H = \frac{u_*}{\bar{u}} \left[\frac{F(|\theta_1 - \theta_2|)}{|\Delta T/\Delta Z|} \right]^{1/2}, \tag{1}$$

where H = height of internal boundary layer (m), u_* = friction velocity over the downwind surface (m s^{-1}), $\bar{u}$ = mean wind speed (m s^{-1}), F = fetch over downwind surface (m), θ_1 = low-level potential air temperature over the source region (°K), θ_2 = temperature of downwind surface (°K), $|\Delta T/\Delta Z|$ = absolute value of the lapse rate over the source region or above the inversion (°K m^{-1}).

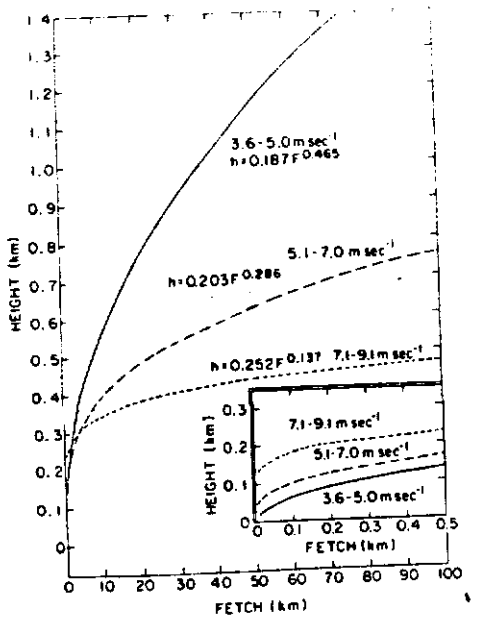

Fig. 11. Change of mean height with fetch for three wind speed classes.

Venkatram (1977) later derived essentially the same model from theoretical considerations. Di Vecchio *et al.* (1976) tested the model with independent data and found similar good agreement for cases with short fetches over land. The model was further tested against data acquired in this study. Some of the input terms such as u_* were not measured directly and had to be estimated from other measurements. Other terms had different averaging times due to the methods of data collection.

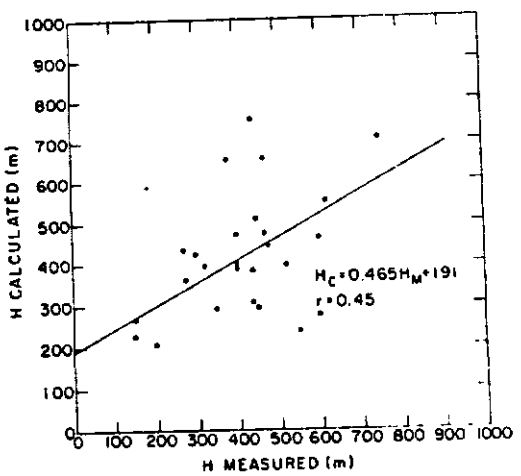

Fig. 12. A comparison of calculated height (H_C) to measured height (H_M).

Despite these problems, the results shown in Figure 12 indicate reasonably good agreement since nearly all predicted heights are within a factor of two of the measured heights. However, the regression line indicates that the model overpredicts heights under 400 m and underpredicts heights above.

4.4. Equilibrium Height

The equations shown in Figures 7–11 predict a continuous rise in the height of the boundary layer although at a decreasing rate, but an equilibrium height is probably reached in all cases except those with free convection. In many runs, the equilibrium height was not determined since traverses were not made to great enough altitudes. In nearly half of the tests, however, a maximum height was reached above which the turbulence level was similar to that over the ocean.

Equilibrium heights ranged from 480 to greater than 900 m and the distances from the coast at which they were reached varied from 5.1 to 40.6 km or greater. No relationship was found between equilibrium height and the distance at which it occurred. No relationship between either height or distance and cloud cover or flow type (sea breeze or gradient) was found. A rather poor inverse relationship was found between wind speed and both equilibrium height and distance. The data suggest that the mean equilibrium height is greater and the distance at which it is reached is less in the summer than in the winter but the data are not adequate to show a functional relationship.

4.5. Temporal Structure

Temperature measurements were plotted as profiles and as cross-sections to show the changes with inland distance and with time. The initial temperature profile over the ocean determined the pattern of change in the transition region as the air moved inland. In most tests, a low-level inversion was present over the ocean since the southerly, onshore winds were typically warmer than the water. In a few cases during the colder months, the air was colder than the water and temperatures over the ocean decreased with height from the surface. In a few runs, water temperature was not measured and the low-level temperature structure could not be determined. In all runs, an adiabatic or superadiabatic lapse rate existed inland during the period of measurement.

During Run BL6, a superadiabatic lapse rate was present over the ocean which was several degrees colder than the land. Air flowing inland (Figure 13) was gradually warmed at the surface and throughout the height of the boundary layer. In this March case, a small inversion which was present above 700 m over the ocean and over the sound to the north was nearly obliterated over the intervening land by the heating from below. Temperature profiles over the ocean and at BNL (Figure 14) show the warming throughout the mixed boundary layer.

During the July run BL3, a low-level inversion was present over the ocean which was much colder than the land. The low-level cold air flow was warmed from below as it moved inland leaving an elevated cool layer between the inversion layer and the

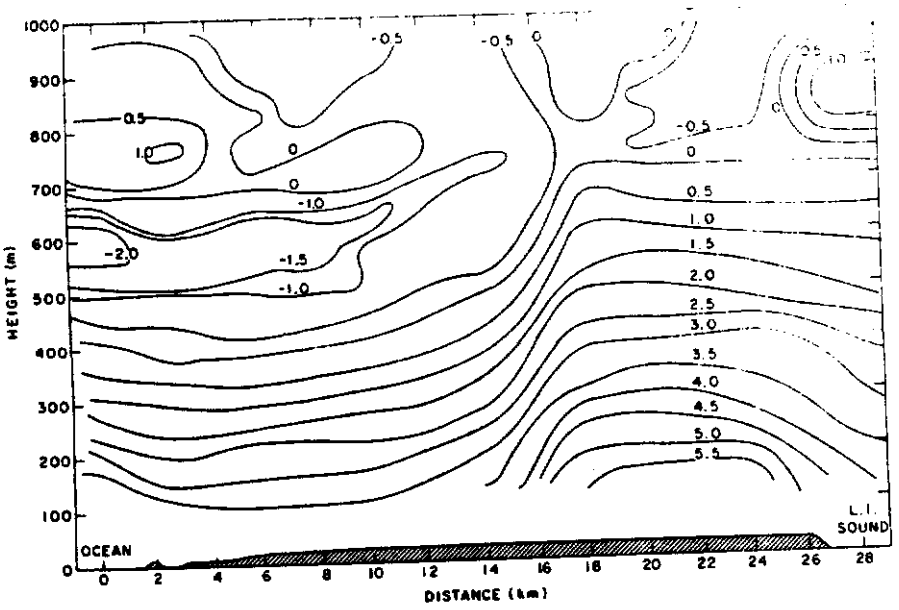

Fig. 13. Temperature cross-section during BL6 with a negative lapse rate over the ocean.

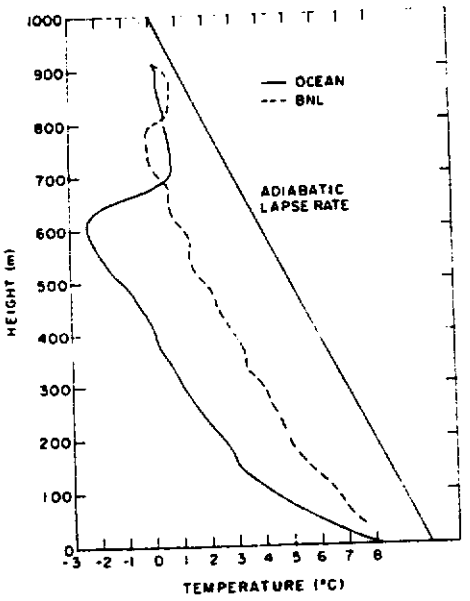

Fig. 14. Temperature profiles over the ocean and inland (BNL) during BL6.

growing internal boundary layer (Figure 15). The cool layer was completely eroded about halfway across the island as the inversion layer merged with the air heated from below over the northern half of the island. Temperature profiles for this case (Figure 16) illustrate the marked warming below with little change above 300 m.

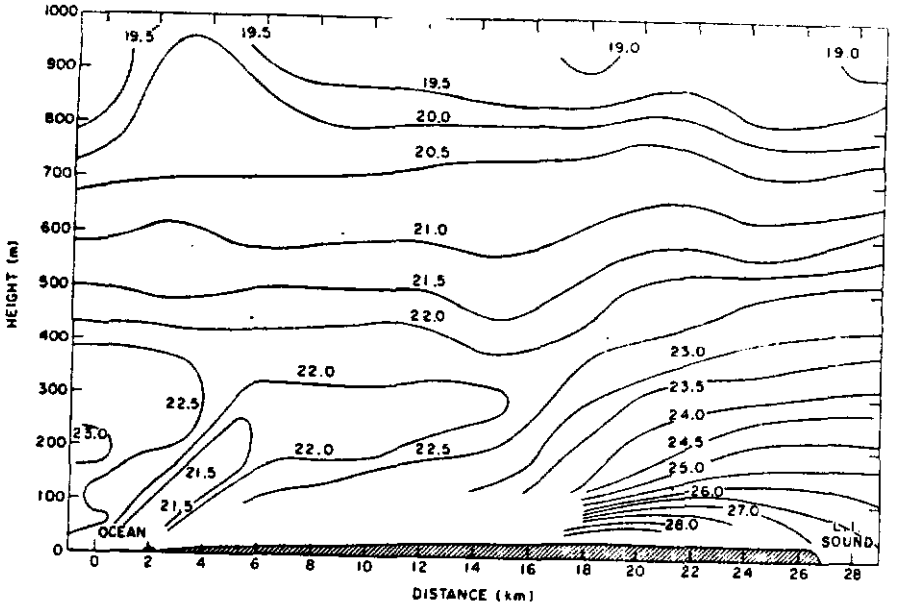

Fig. 15. Temperature cross-section during BL3 with a low level inversion over the ocean.

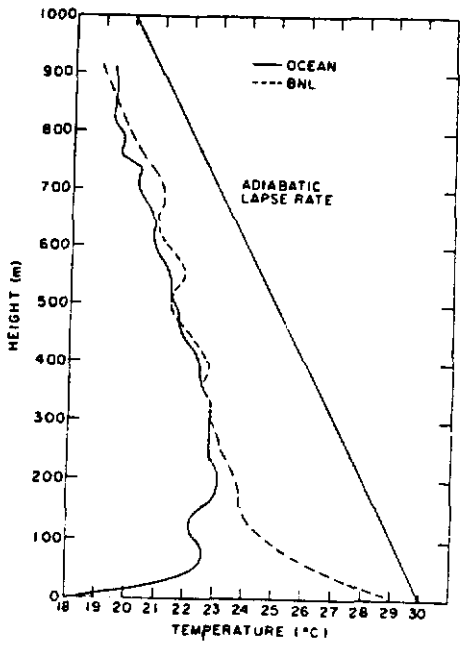

Fig. 16. Temperature profiles over the ocean and inland (BNL) during BL3.

One test (BL8) was made in November with the water temperature approximately equal to that of the land. Profiles were close to adiabatic over both land and water. No heating took place as the air moved inland and the isotherms remained essentially horizontal throughout the entire cross-section.

The temperature structure during a well-developed sea breeze is shown in Figure 17. The strong temperature discontinuity marks the sea breeze front and is at the seaward edge of the chimney of heavy turbulence shown in Figure 5. Temperatures behind the front are much warmer than those in the marine air even though warming had occurred near the surface as the air moved inland.

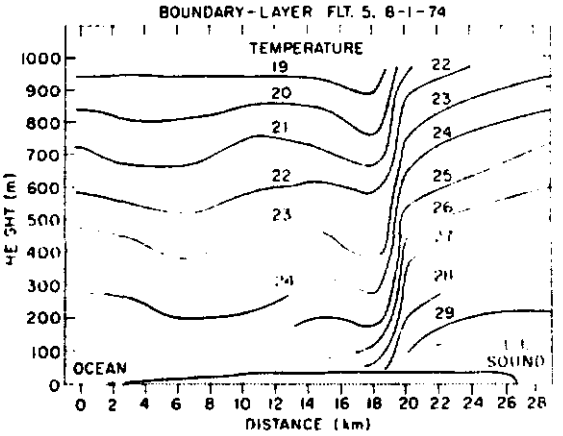

Fig. 17. Temperature cross-section during BL5 with a strong sea breeze flow.

These four cases represent the range of conditions sampled. Temperature changes in other tests were similar.

4.6. Wind above surface

During onshore flows, wind speeds over the ocean typically have one or more maxima at relatively low altitudes (Figure 18). Winds inland usually show a similar pattern although the height of the peak may differ and its magnitude is usually less. If the winds inland are from other directions, the low-level maximum is usually absent. This is also illustrated in Figure 18 where the 1139 BNL wind profile was taken shortly before the arrival of a sea breeze and the 1230 profile in a well developed sea breeze. Differences in direction between the coast and inland are usually small except when a sea-breeze front separates the two locations.

The average magnitude and average height of the low-level wind speed maximum was determined for each boundary-layer test in which flow was onshore and in which complete sets of pilot balloon soundings were taken at the coast and at BNL. The magnitudes of the peaks were related to the surface (11 m) wind speeds at each

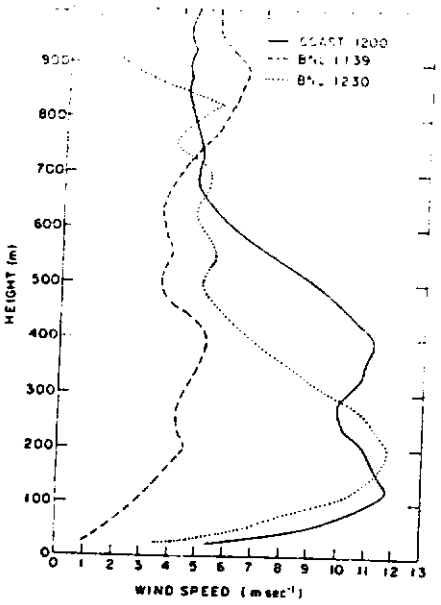

Fig. 18. Wind-speed profiles at the coast and at BNL before and after the passage of a sea breeze front showing the inland penetration of a low level wind speed maximum.

location and the magnitude and height of the peak inland were related to those at the coast. Data are given in Table V.

As shown by the ratios, peak speeds at both locations averaged about twice the surface speeds but ranged from 1.4 to 2.4 at the coast and from 1.6 to 3.5 inland. The somewhat larger average ratio inland results from the fact that the peak speed does not decrease as much with inland distance as the surface speed.

The ratio of the peak speed inland to that at the coast ranges from 0.5 to 0.8 and averages 0.71. The comparable mean ratio of surface speeds (not tabulated) is 0.68. The ratio of the height of the peak inland to the height at the coast varies from 0.7 to 1.6 and averages 1.05. Thus, the peak may either rise or descend as it penetrates inland but is usually from 150–200 m above the surface at both locations.

The behavior of the wind-speed maximum was also examined as a function of time during each test. The height of the peak usually fluctuated with time at both locations. In a few cases, the peak ascended with time and another formed below near the original elevation. The magnitude of the peak also varied with time but usually reached a maximum in early afternoon at the time of highest land surface temperature.

In most cases, the wind-speed maximum was found below the top of the boundary layer inland. At the coast, it most often occurred below the inversion top when one was present. Higher-level wind speed maxima often occurred also and seemed unrelated to the internal boundary layer or to inversion layers.

TABLE V

Summary of surface and peak wind speeds at coast and BNL and their ratios

Test no.	Date	Coast			BNL			Peak/Surface Wind Speed Ratio		Inland/Coast Ratios	
		Speed Surface ($m\,s^{-1}$)	Speed Peak ($m\,s^{-1}$)	Ht. Peak (m)	Speed Surface ($m\,s^{-1}$)	Speed Peak ($m\,s^{-1}$)	Ht. Peak (m)	Coast	BNL	Peak Speed	Ht. of Peak
BL3	7-2-74	7.0	15.6	170	5.2	9.8	221	2.23	1.88	0.63	1.30
BL5	8-1-74	6.3	12.3	147	4.8	9.0	199	1.95	1.87	0.73	1.35
BL6	3-18-75	4.5	8.8	218	4.0	6.2	191	1.95	1.55	0.75	0.88
BL8	11-12-75	6.1	8.8	136	3.9	6.9	180	1.44	1.76	0.78	1.32
BL9	3-19-76	7.2	17.5	170	5.2	9.0	130	2.43	1.73	0.52	0.77
BL10	6-24-76	7.2	12.5	120	4.4	10.5	205	1.73	2.40	0.84	1.64
BL11	7-27-76	7.4	15.1	244	2.9	10.2	181	2.03	3.52	0.68	0.74
Mean		6.55	12.90	173	4.35	8.83	187	1.97	2.11	0.71	1.05

4.7. Change in Higher-Level Turbulence

Quantitative measurements of the vertical component of turbulent velocity fluctuations, σ_w, were obtained by use of the variometer during fourteen flights in which data were recorded. Each horizontal pass was divided into segments within and outside of the internal boundary layer and mean values of σ_w calculated for each segment. Results are given in Table VI.

TABLE VI

Measurements of vertical velocity (σ_w) in m s^{-1} by height within and outside of internal boundary layer with number of cases

Height (m)	Outside of B.L.				Within B.L.			
	Mean	Min.	Max.	n	Mean	Min.	Max.	n
152	0.166	0.075	0.303	8	0.926	0.606	1.029	9
183	0.452	0.335	0.650	4	1.221	0.990	1.431	4
213	0.338	0.238	0.438	2	0.916	0.506	1.325	2
244	0.289	0.131	0.538	9	1.098	0.856	1.425	8
274	0.234	0.094	0.550	6	0.850	0.425	1.156	7
305	—	—	—	—	0.913	0.913	0.913	1
335	0.261	0.063	0.525	8	0.927	0.676	1.157	9
366	0.250	0.137	0.500	5	0.704	0.244	0.990	5
391	—	—	—	—	1.325	1.325	1.325	1
427	0.221	0.128	0.377	6	0.884	0.744	1.017	6
457	0.188	0.092	0.361	5	0.812	0.769	0.838	4
488	0.350	0.350	0.350	1	0.831	0.831	0.831	1
518	0.237	0.094	0.609	7	0.676	0.365	1.110	6
549	0.232	0.151	0.327	5	0.820	0.613	1.131	4
610	0.236	0.119	0.474	6	0.794	0.450	1.056	5
640	0.215	0.135	0.299	4	0.759	0.472	1.007	3
701	0.159	0.088	0.246	5	0.491	0.311	0.694	3
732	0.255	0.138	0.309	4	0.730	0.445	1.112	3
762	0.163	0.163	0.163	1	0.175	0.175	0.175	1
792	0.296	0.223	0.390	3	0.892	0.892	0.892	1
823	0.227	0.167	0.334	3	1.420	0.520	0.900	2
914	0.218	0.204	0.231	2	0.700	0.564	0.845	2

Outside of the internal boundary layer (upwind and above), σ_w averaged 0.243 m s^{-1} and showed only a slight tendency to decrease with height. σ_w averaged somewhat larger when lapse rates over the ocean were unstable or neutral than during stable cases but differences with stability were small.

Within the internal boundary layer, σ_w averaged 0.855 over all heights and showed a somewhat greater tendency to decrease with height. However, the large amount of scatter precluded establishing any systematic relationship. Since all data were taken during the day, lapse rates over the land were all unstable or neutral and no classification of cases by lapse rate was possible. No relationship was found

between σ_w and season, wind speed, wind direction or cloudiness although some such relationship might be expected with a larger number of cases.

Ratios of σ_w within the internal boundary layer to σ_w outside it during a single pass at a constant height showed a great deal of scatter but averaged 3.52 for all cases. Thus, vertical velocity, and presumably vertical diffusion, averaged three to four times greater within the internal boundary layer than upwind or above.

Successful measurements of the energy dissipation rate, ε, were obtained on only the last two runs. The value of ε showed a systematic decrease with height within the internal boundary layer. In one run (BL10) the mean value of ε within the boundary layer decreased from 30 $cm^2 s^{-3}$ at 183 m to 3 $cm^2 s^{-3}$ at 732 m and ranged from 0.08 to 0.32 $cm^2 s^{-3}$ upwind of and above the internal boundary layer. In run BL11, ε decreased from 51 $cm^2 s^{-3}$ at 183 m to 9.7 $cm^2 s^{-3}$ at 640 m. In this case, values outside of the boundary layer were somewhat larger than in BL10, from 0.40 to 1.04 $cm^2 s^{-3}$. These preliminary results suggest that the energy dissipation rate decreases with height at a faster rate than σ_w within the internal boundary layer and that differences between ε in the modified air and ε in the unmodified air are greater than differences in σ_w. This is expected since ε is proportional to u_*^3 and σ_w is approximately equal to u_*.

4.8. Change in low-level turbulence

The differences in low-level turbulence within and outside of the internal boundary layer were investigated in 18 test periods with onshore flows. Sensitive bivanes were operated simultaneously at 23 m above the ground on Tiana tower at the coast and on the meteorology tower inland at BNL. Results presented in Table VII show large differences in each measure of turbulence between the two locations. Although mean wind speed ($\bar{u}$) averages appreciably less inland, the standard deviation of the speed fluctuations (σ_u) and the turbulence level ($\sigma_u/\bar{u}$) average several times greater. Both lateral and vertical direction fluctuations (σ_θ and σ_ϕ) are over an order of magnitude greater inland. These tests were all made during daylight hours between April and September. Smaller differences would be expected at night when the air inland is more stable and during the colder months when the air over the ocean is less stable.

4.9. Change in surface wind speed

During onshore flows, 11-m wind speeds at BNL located about 17 km from the coast and well within the internal boundary layer nearly always averaged appreciably less than those at the coast. Ratios during all boundary-layer tests varied from 0.15 to 1.00. The mean was 0.68 and the standard deviation 0.19. The ratio was examined as a function of fetch along the wind from the coast to the inland location and of coastal wind speed but consistent relationships were not found.

A year of hourly climatological data from the station at Smith's Point on the coast and Brookhaven Airport 9 km inland gave a mean wind speed ratio of 0.72 during onshore flow periods. These more extensive data suggest that the ratio is greatest with low speeds at the coast and least with higher speeds. In other words, speeds

TABLE VII

Simultaneous coastal and inland turbulence measurements at 23 m above the ground with their ratios

Test	Date	Time	Coast					Inland					Ratio Inland/Coast				
			$\bar{u}$ (ms^{-1})	σ_u (ms^{-1})	$\sigma_u/\bar{u}$	σ_θ (deg)	σ_ϕ (deg)	$\bar{u}$ (ms^{-1})	σ_u (ms^{-1})	$\sigma_u/\bar{u}$	σ_θ (deg)	σ_ϕ (deg)	$\bar{u}$	σ_u	$\sigma_u/\bar{u}$	σ_θ	σ_ϕ
W31	4-13-77	1157–1313	8.99	0.45	0.05	2.90	0.70	4.20	1.79	0.43	13.00	13.70	0.47	3.98	8.52	4.5	19.6
		1313–1413	8.76	0.34	0.09	2.30	0.90	5.60	1.88	0.34	10.20	13.70	0.64	5.53	8.62	4.4	15.2
W32	5-17-77	1310–1410	10.55	0.85	0.08	2.70	0.90	5.60	1.25	0.22	119.00	10.80	0.53	1.47	2.75	44.1	12.0
		1410–1510	10.95	0.52	0.05	2.30	0.80	6.10	1.52	0.25	77.00	8.60	0.56	2.92	5.30	33.5	10.8
W33	5-18-77	1200–1300	7.14	1.08	0.15	4.60	1.00	2.24	0.34	0.15	77.43	12.82	0.31	0.31	1.01	16.8	12.8
		1300–1400	8.49	1.58	0.19	11.10	2.30	1.90	0.43	0.23	86.93	11.27	0.22	0.27	1.22	7.8	4.9
W34	5-24-77	1045–1145	6.79	0.16	0.02	0.54	0.42	4.62	1.45	0.31	18.91	13.04	0.68	9.06	13.08	35.0	31.1
		1145–1245	—	—	—	—	—	4.90	1.41	0.29	20.20	13.60	—	—	—	—	—
W35	5-31-77	1355–1455	6.04	0.61	0.10	4.58	1.75	4.68	1.59	0.34	23.57	14.37	0.77	2.61	3.37	5.1	8.2
		1455–1555	5.70	1.16	0.20	6.83	1.77	4.92	2.89	0.59	10.91	36.90	0.86	2.49	2.88	1.6	20.8
W36	6-16-77	1333–1433	6.80	0.97	0.14	3.34	0.60	5.27	1.65	0.31	48.50	9.90	0.78	1.70	2.19	14.5	16.5
		1433–1533	6.66	1.79	0.27	6.04	0.42	—	—	—	—	—	—	—	—	—	—
W37	7-20-77	1245–1345	6.33	0.98	0.16	5.22	0.95	3.23	1.06	0.33	45.16	17.28	0.51	1.08	2.12	8.7	18.2
		1345–1445	7.32	1.59	0.22	20.30	0.80	2.45	1.52	0.62	89.84	23.18	0.33	0.96	2.84	4.4	29.0
W38	7-25-77	0900–1000	14.05	0.87	0.06	3.15	1.70	—	—	—	11.59	11.25	—	—	—	3.7	6.6
		1000–1100	13.81	0.95	0.07	3.54	1.76	—	—	—	12.17	12.69	—	—	—	3.4	7.2
W39	9-13-77	0905–1005	9.77	0.73	0.08	21.30	7.48	7.63	1.63	0.21	33.90	12.90	0.78	2.23	2.86	1.6	1.7
		1005–1105	9.52	0.72	0.08	4.04	1.26	6.12	1.58	0.26	18.80	12.40	0.64	2.44	3.39	4.7	9.8
Mean[a]			8.08	0.84	0.12	6.58	1.55	4.61	1.47	0.33	48.08	15.06	0.58	2.65	4.23	13.3	15.0

[a] The mean includes only those 14 test periods for which complete data were obtained.

within the boundary layer inland tend to remain relatively constant despite changes at the coast. Another limited data set showed that coastal and inland sites had nearly equal wind speeds when the speed at the coast was 2 m s^{-1} but when the speed at the coast increased to 8 m s^{-1}, the speed inland increased to only 4 m s^{-1}.

4.10. Change in surface wind direction

Change in wind direction between the coast and BNL was examined for the boundary-layer flight periods. When the wind approached the shore nearly normal to the coastline, the direction inland was almost identical. When the wind approached the coast at an angle, however, the inland direction was almost always more nearly normal to the coast indicating curvature, either clockwise or counterclockwise as the flow moved inland. In other words, both southeast and southwest winds at the coast became more southerly inland. This change in direction is believed to be due to the increased frictional drag inland and to the local pressure gradient between the air over the heated land and that over the cooler water. This phenomena will be examined with more extensive data and results presented later.

5. Discussion

Peterson's (1969) model predicts the growth of the internal boundary layer (h) as $h \sim F^{0.8}$ where F is the fetch. Peterson also gives a nomogram in which the non-dimensional height of the interface, h/z_0, is given as a function of the non-dimensional downwind distance, F/z_0, for different $m = \ln(z_0'/z_0)$, where z_0' and z_0 are the roughness lengths upwind and downwind, respectively. Typically $z_0' \simeq 0.001$ m and $z_0 \simeq 1$ m for these experiments; hence for $m < 0$, a value for h of about 1000 m was obtained for a fetch of 10 km. Our observations indicate a height of 300 to 500 m depending on the range of wind speeds (Figure 10). This over-prediction by the model is probably due to: (1) stable upwind atmospheric conditions in our experiments and, (2) use of the model beyond its range of validity. Internal boundary layers are known to be steeper near the origin of the change in roughness. Peterson's $F^{0.8}$ relationship agrees with previous results of boundary-layer height variation near the interface (Elliott, 1958; Panofsky and Townsend, 1964). Results of the present experiments indicate that this slope is not the same for larger downwind distances and it is affected strongly by upwind and downwind stability conditions. It has been observed at least qualitatively in wind tunnels that the internal boundary layers grow at a slower rate for surface-based inversions upwind as compared with neutral conditions (SethuRaman and Cermak, 1975). In this study the airflow was from smooth to rougher surface and the downwind stability conditions were unstable. A direct comparison of the present data with Taylor's results is not feasible since his numerical models were not designed for large downwind distances.

Some practical applications of this study are evident. Emission of air pollutants from a coastal source at a height above the internal boundary layer during onshore flows may result in prolonged periods of fumigation with resultant high surface

concentrations. Similar releases with offshore flows may remain above the more shallow stable boundary layer over the water but fumigation would be expected if the plume passed over a body of water to another land mass. Emission into the unstable boundary layer with onshore flows would also result in higher than expected concentrations since vertical diffusion is limited by the stable layer aloft which is often considerably lower than the height of the mixed layer at inland locations. Diurnal changes in mixing-layer height and in diffusion rate may be much smaller at the coast than in typical inland locations.

6. Conclusions

Internal boundary layers typically develop at coastlines because of differences in temperature and roughness between the upwind and downwind surfaces. The modified and unmodified air differ in turbulence and wind speed and sometimes in wind direction. Average slope of the internal boundary layer is steep (~1 : 4) close to the interface and shallow (~1 : 100) at greater distances. In the absence of free convection or a sea breeze return flow, an equilibrium height is usually reached. The height of the boundary layer is inversely related to wind speed but correlated with temperature difference between the two surfaces. Near the interface, the lapse rate over the upwind surface influences the slope which is shallower with stable air and steeper with neutral and unstable lapse rates upwind. Models developed for predicting height at small downwind distances are not applicable to the distances and height intervals studied but reasonably good predictions are given by an empirical model.

Acknowledgements

This study was made possible by the assistance of many individuals both in field operations and data analyses. Many of the aircraft flights were made by W. Ansel Tuthill and others by John McNeil and Seymour Fink. Walter Jahnig took much of the pilot balloon data. Catherine Henderson assisted in much of the data analysis.

The submitted manuscript has been authored under contract EY-76-C-02-0016 with the U.S. Department of Energy. Accordingly, the U.S. Government retains a nonexclusive, royalty-free license to publish or reproduce the published form of this contribution, or allow others to do so, for U.S. Government purposes.

References

Collins, G. F.: 1974, 'Predicting "Sea-Breeze Fumigation" from Tall Stacks at Coastal Locations', *Nuclear Safety* 12, 110–114.

Di Vecchio, R. A., Smith, D. B., and Martin, G.: 1976, 'Performance of a Recent Formulation for Rate of Growth of Boundary Layers near Shorelines', Presented *Amer. Meteorol. Soc. Conf. on Coastal Meteorology*, Sept. 21–23, Virginia Beach, Va.

Dooley, J. C., Jr.: 1976, 'Fumigation from Power Plant Plumes in the Lakeshore Environment', Report No. 18, Air Pollution Analysis Laboratory, Univ. of Wisconsin-Milwaukee, 119 pp.

Echols, W. T. and Wagner, N. K.: 1972, 'Surface Roughness and Internal Boundary Layer near a Coastline', *J. Appl. Meteorol.* **11**, 658–662.

Elliott, W. P.: 1958, 'The Growth of the Atmospheric Internal Boundary Layer', *Trans. Amer. Geophys. Union* **39**, 1048–1054.

Hewson, E. W. and Olsson, L. E.: 1967, 'Lake Effects on Air Pollution Dispersion', *J. Air Poll. Control Assn.* **17**, 757–761.

Lyons, W. A. and Cole, H. S.: 1973, 'Fumigation and Plume Trapping on the Shores of Lake Michigan during Stable Onshore Flow', *J. Appl. Meteorol.* **12**, 494–510.

Lyons, W. A. and Olsson, L. E.: 1972, 'Mesoscale Air Pollution Transport in the Chicago Lake Breeze', *J. Air Poll. Control Assn.* **22**, 876–881.

Panofsky, H. A. and Townsend, A.: 1964, 'Change of Terrain Roughness and the Wind Profile', *Quart. J. Roy. Meteorol. Soc.* **90**, 147–155.

Peterson, E. W.: 1969. 'Modification of Mean Flow and Turbulent Energy by a Change in Surface Roughness under Conditions of Neutral Stability', *Quart. J. Roy. Meteorol. Soc.* **95**, 561–575.

Prophet, D. T.: 1961, 'Survey of the Available Information Pertaining to the Transport and Diffusion of Airborne Material over Ocean and Shoreline Complexes', Tech. Report No. 89, Aerosol Laboratory, Stanford Univ., Stanford, Cal., 53 pp.

Raynor, G. S., Michael, P., Brown, R. M. and SethuRaman, S.: 1975, 'Studies of Atmospheric Diffusion from a Nearshore Oceanic Site', *J. Appl. Meteorol.* **14**, 1080–1094.

Raynor, G. S.: 1977, 'Effects on Atmospheric Diffusion of Meteorological Processes in Coastal Zones', Presented ASTM Conf. on Air Quality Meteorology and Atmospheric Ozone, August 1–6, Boulder, Colo. Report BNL 22815, Brookhaven National Laboratory, Upton, N. Y.

Raynor, G. S., Brown, R. M., and SethuRaman, S.: 1978, 'A Comparison of Diffusion from a Small Island and an Undisturbed Ocean Site', *J. Appl. Meteorol.* **17**, 129–139.

SethuRaman, S., Brown, R. M., Raynor, G. S., and Tuthill, W. A.: 1979, 'Calibration and Use of a Sail Plane Variometer to Measure Vertical Velocity Fluctuations', *Boundary-Layer Meteorol.* **16**, 99–105.

SethuRaman, S. and Cermak, J. E.: 1975, 'Mean Temperature and Mean Concentration Distributions over a Physically Modelled Three-dimensional Heat Island for Different Stability Conditions', *Boundary-Layer Meteorol.* **9**, 427–440.

Taylor, P. A.: 1969a, 'On Planetary Boundary Layer Flow under Conditions of Neutral Thermal Stability', *J. Atmos. Sci.* **26**, 427–431.

Taylor, P. A.: 1969b, 'The Planetary Boundary Layer above a Change in Surface Roughness', *J. Atmos. Sci.* **26**, 432–440.

Taylor, P. A.: 1969c, 'On Wind and Shear Stress Profiles above a Change in Surface Roughness', *Quart. J. Roy. Meteorol. Soc.* **95**, 77–91.

Taylor, P. A.: 1970, 'A Model of Airflow above Changes in Surface Heat Flux, Temperature and Roughness for Neutral and Unstable Conditions', *Boundary-Layer Meteorol.* **1**, 18–39.

Taylor, P. A.: 1971, 'Airflow above Changes in Surface Heat Flux, Temperature and Roughness: An Extension to Include the Stable Case', *Boundary-Layer Meteorol.* **1**, 474–497.

Van der Hoven, I.: 1967, 'Atmospheric Transport and Diffusion at Coastal Sites', *Nuclear Safety* **8**, 490–499.

Venkatram, A.: 1977, 'A Model of Internal Boundary Layer Development', *Boundary-Layer Meteorol.* **11**, 419–437.